On the use of infinite elements for the determination of optimal closure patterns based on stress analysis

D. A. Lott[(1)] **and H. R. Chaudry**[(2)]

[(1)] Department of Mathematical Sciences and
Center for Applied Mathematics and Statistics
New Jersey Institute of Technology, Newark, NJ 07102

[(2)] Department of Biomechanical Engineering
New Jersey Institute of Technology, Newark, NJ 07102 and
V.A. Medical Center, East Orange, NJ

CAMS Report 0203-05, Fall 2002

Center for Applied Mathematics and Statistics

NJIT

On the use of infinite elements for the determination of optimal closure patterns based on stress analysis

D. A. Lott[1] and H. R. Chaudhry[2]

Abstract

Solid infinite elements are used in conjunction with finite elements to compute the stress and displacement distribution resulting from the suturing of wounds of symmetric and nonsymmetric shapes in orthotropic, abdominal human skin. The optimal pattern of suturing of wounds are investigated from a stress perspective. Highly accurate, quantitative and qualitative improvements over the use of finite elements to approximate distant boundaries are obtained. Numerical results quantitatively agree with analytic results computed using complex analysis techniques. The technique used and the results obtained will aid surgeons in closing nonsymmetrical wounds on regions of the body that exhibit orthotropy.

Key words: Infinite elements, stress, wounds, orthotropy, skin

1 Introduction

Stress is one of the many biological factors that plays an important role in wound healing, granulation and scar production [1, 2, 3]. The most important quantity in determining how a wound will heal is the maximum stress acting upon it [4] since maximum stresses have adverse effects on wound healing [1]. Any numerical technique used to analyze stresses around the wound closure should qualitatively and quantitatively predict the true stresses. Such a noninvasive, numerical technique will aid surgeons in the determination of stresses as a result of suturing.

Several researchers have proposed theoretical models to develop the constitutive equation for the skin [5, 6]. These models support the evidence of a nonlinear stress-strain relationship to model the mechanics of skin deformation; however, they neglect the effects of shear strains which are present in all suturing models. Other researchers have modelled the suturing of wounds using the finite element method [7, 8, 9] and have suggested optimal suturing patterns for closure based on reliable qualitative analysis. It was done using conformal mapping and complex variable techniques [10] as well as the finite element technique only [9]. In the analytical technique, the wound is assumed to be symmetric which in practice, is not the case [10]. Thus the solution by complex analysis is deficient in considering wounds of nonsymmetric boundary although this technique makes use of an infinite boundary for the skin sheet. Numerical techniques which employ the finite element method artificially assume placement of the boundary of the skin sheet

[1]Department of Mathematical Sciences, Center for Applied Mathematics and Statistics, New Jersey Institute of Technology, Newark, NJ 07102, (973) 642-7807 (p), *dalc@dalc.njit.edu*

[2]Department of Biomechanical Engineering, New Jersey Institute of Technology, Newark, NJ 07102, (973) 642-7835 (p), *chaudhry@m.njit.edu* and V.A. Medical Center, East Orange, New Jersey

and impose displacement boundary conditions that vanish [9]. Hence, this computational method is deficient in imposing boundary conditions in infinite dimensions. The finite element technique requires experimentation with mesh sizes and assumed boundary conditions which may not accurately simulate stresses and displacement at the truncated edges [11]. It is computationally expensive to enlarge the numerical mesh by placing the truncation boundary far away from the wound itself. Although placing the truncation boundary too close to the wound saves computational time, influential stresses which lie outside the truncation boundary are neglected. As a result, vital quantitative information is lost. Although qualitatively correct, the finite element method does not provide the quantitative accuracy necessary for clinical application since displacements at an assumed distance from the wound physically do not vanish. Hence, the stresses that occur as a result of the imposed boundary conditions are not, in fact, correct. Physical stresses and displacements should die out as the radial distance away from the wound increases and this phenomenon should be modelled naturally. From a physiological point of view, it is necessary to provide an accurate stress analysis, apart from, predicting the optimal suturing pattern.

We therefore improve upon our previous work by simulating the suturing of a wound in an *unbounded domain* under the assumption that the area of skin affected by suturing is also influenced by the deformations in the surrounding medium, away from the wound. Therefore, we employ the use of infinite elements in the far field to increase accuracy in the stress computation. Use of infinite elements allows the modelling of effects in the far-field to decay without having to specify vanishing boundary conditions at the "edge" of the computational region.

Over the past few years, infinite elements have become a popular method of exterior approximation in scattering problems [12]. In particular, the use of acoustic infinite elements has exhibited many advantages, foremost among them being very high computational efficiency, convergence and, as a result, unlimited accuracy throughout the entire fluid domain [13]. Infinite elements have been employed for the analysis of hydrodynamic loads on offshore structures [14]. Optimal dielectric waveguides have been modelled with finite elements in conjunction with edge infinite elements [15]. Other areas where infinite elements have been applied include soil-structure interactions [16, 17], problems with non-reflecting boundary conditions, inverse scattering methods, applications to exterior field problems [18], coupling field problems [19, 20], and open boundary problems [21].

The previous works pertaining to infinite elements suggest that the use of infinite elements would greatly improve the efficiency, convergence and accuracy of the solution near the wound closure line and in the outer regions of the skin sheet. In this paper, the model problem is the determination of optimal patterns for suturing wounds of the same area but different complex geometries to obtain careful and accurate quantitative results. In particular, average principal stresses are computed and compared to determine an invariant numerical mesh which predicts optimal closure patterns.

The mathematical model and the numerical method are presented in Section 2. In Section 3, all numerical results are presented. Sections 4 and 5 are the Discussion and Conclusion, respectively.

2 Method

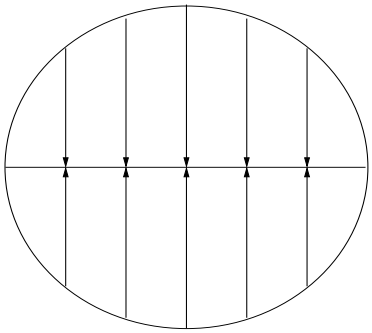

Figure 1a: Geometry of suturing a circular wound vertically toward the x-axis

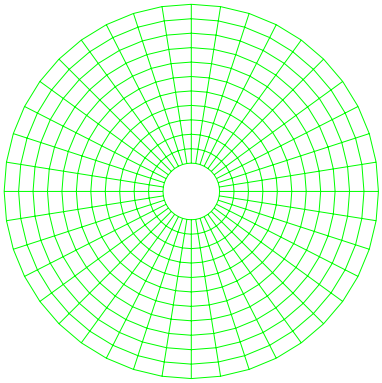

Figure 1b: Control region Ω_0 for the circular wound of area 9.4×10^{-4} m^2. Deformed area of Ω_0 is 4.00315×10^{-2} m^2.

We consider three problems for the sake of illustration. In the first problem, a circular wound of area 9.4×10^{-4} m^2 is sutured vertically toward the x-axis (Fig 1a). We use this symmetric suturing pattern to demonstrate the accuracy of the solution computed by finite and infinite elements as compared to those solutions computed using finite elements only [9]. We divide the solution of this problem into two parts. The first part of this problem consists of modelling the suturing process in a domain Ω_k with truncated edges and is approximated by finite elements only. We define the control region, Ω_0, as the local area surrounding the wound on which all calculations of stress for different simulations are computed. For the circular wound, the control region of stress calculation is a circular area of 4.00315×10^{-2} m^2 (deformed) enclosing the wound (Fig 1b). This region, Ω_0, is approximated by a mesh consisting of 440 four node isoparametric finite elements arranged in 11 radially concentric annuli each of 40 elements, circumscribing the wound.

For this purpose, the software package, ABAQUS [11], utilizing the finite element method (FEM) is used to determine the stresses numerically for sutured wounds of complex shapes *in vivo*. Elements are chosen to be of type CPS4; that is, continuum plane stress quadrilateral elements [11]. For the first simulation, zero displacement boundary conditions are imposed on the boundary of Ω_0. Wound closure is simulated and the average principal stresses are computed within the region Ω_0. For the second simulation, a larger region, Ω_1, containing Ω_0, is defined consisting of a mesh of 560 four node isoparametric elements, arranged in 14 radially concentric annuli, each of 40 elements. Note that the inner 11 radial components comprise Ω_0. Wound closure is again simulated and the average principal stresses are computed within the region Ω_0. For the i^{th} simulation on a truncated region Ω_i, $i = 1, 2, \ldots N$, enclosing the control region Ω_0, the radius of Ω_i is increased to simulate finite approximations on a successively larger skin sheet. That

is, four node isoparametric finite elements are arranged in radially concentric annuli each of 40 elements of increasing radial length (of elements), thereby increasing the area of the computational region. In each test, we assume the stresses die out by imposing zero displacements at the boundary of Ω_i and compute average principal stresses within the region Ω_0.

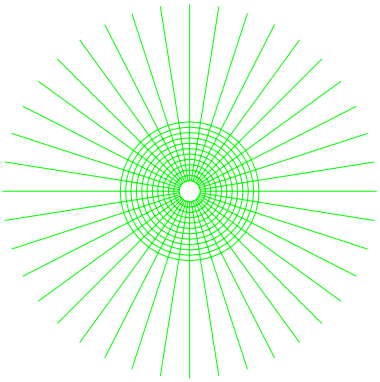

Figure 2: Computational mesh of 440 four node isoparametric CPS4 finite elements is surrounded by 40 CINPS4 infinite elements for the circular wound. Area of the circular wound is 9.4×10^{-4} m^2. The center region Ω_0 has deformed area of 4.00315×10^{-2} m^2.

In the second part of this problem, infinite elements are used in conjunction with standard finite elements. Finite elements mesh the area around the region of interest and infinite elements mesh the area in the far field region (Fig 2).

In both parts, the assumption is that the region of highest stresses is considerably small and the stresses and displacements die out radially away from the suture line. Infinite elements are used on the perimeter of the truncated region Ω_i to approximate the far field region. In all simulations, the far field region is approximated by a mesh containing 40, 4 node isoparametric infinite elements as a bounding radial layer. Nodes on the boundary of Ω_i define an interface between finite and infinite elements.

In the second problem, an elliptical shape wound of the same area, 9.4×10^{-4} m^2, is sutured vertically toward its major axis (the x-axis) to compare numerical results employing infinite elements with that of published analytical results [10]. (Figures have been omitted due to space limitations but are geometrically similar to figures for the circle). For the elliptical wound, the control region of stress calculation is an elliptical area of 4.00315×10^{-2} m^2 (deformed) enclosing the wound. This region, Ω_0, is approximated by a mesh consisting of 440 four node isoparametric finite elements arranged in 11 radially concentric annuli each of 40 elements, circumscribing the wound. This problem is solved using both finite and infinite elements.

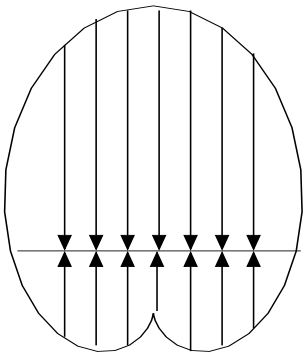

Figure 3a: Geometry of suturing a wound of cardioid shape vertically toward the x-axis

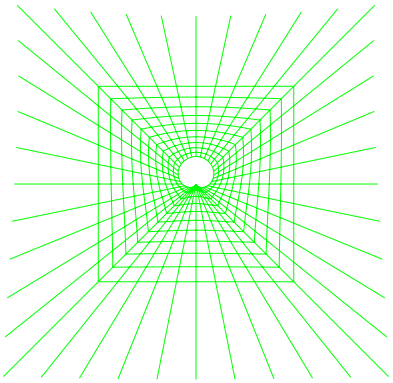

Figure 3b: Computational mesh of 360 four node isoparametric CPS4 finite elements in the center region Ω_0, surrounded by 40 CINPS4 infinite elements for the cardioid wound. Area of the cardioid wound is 9.4×10^{-4} m^2. Area of the rectangular region Ω_0 has deformed area of 3.9067704×10^{-2} m^2.

In the third problem, we choose a nonsymmetrical shaped wound in the form of a cardioid of area 9.4×10^{-4} m^2 to be sutured toward the x-axis to investigate the accuracy of the technique on a wound of complex geometry (Fig 3a). Since the cardioid is nonsymmetric with respect to the x-axis, it is necessary to determine the location of the suture line which results in minimal principal stresses. In addition, we suture a circular and an elliptical wound, as in problems one and two; however, here all three simulations are now calculated on a square control region, Ω_0 of area 0.4 m^2 (Fig 3b). We verify the accuracy of solutions by comparing them with analytic results and determine the optimal pattern of suturing based on the new numerical method. It has been shown that the elliptical geometry is the optimal pattern of closure based on the magnitudes of the principal stresses [9, 10]. Also, optimal patterns of wounds of the same area correspond to ellipses with aspect ratios of 3:1. We hypothesize that these numerical results will compare quantitatively to previously reported results.

We formulate the model problems to be solved from the basic equations of classical elasticity theory for an orthotropic material for plane stress problems. A complete mathematical analysis of the biomechanics of skin requires a system which includes a three-dimensional constitutive equation; however, we take two-dimensional constitutive equations to model the deformation of skin as in [9, 10, 22].

Human skin is known to have a nonlinear stress-strain relationship [8], to exhibit orthotropic and viscoelastic behavior [23, 24, 25], has residual stresses [6, 22], and takes large deformation [4]. In particular, a fully nonlinear stress-strain model for human, abdominal, skin does not exist at this time, however, a three-dimensional model which incorporates

viscoelasticity has been found for facial skin and SMAS (Superficial Musculoaponeurotic System) [26]. Consequently, it is extremely difficult analytically and numerically to take into account all aspects for abdominal human skin. Therefore, we employ a linear stress-strain relationship with nonlinear strain components for orthotropic materials for an *in vivo* configuration in which the elastic parameters for abdominal human skin were determined experimentally by Reihsner et al. [22]. This linear stress-strain relationship is given below:

$$\begin{pmatrix} \sigma_{11} \\ \sigma_{22} \\ \tau_{12} \end{pmatrix} = \begin{pmatrix} E_1/(1-\nu_1\nu_2) & E_1\nu_2/(1-\nu_1\nu_2) & 0 \\ E_2\nu_1/(1-\nu_1\nu_2) & E_2/(1-\nu_1\nu_2) & 0 \\ 0 & 0 & 2G \end{pmatrix} \begin{pmatrix} \epsilon_{11} \\ \epsilon_{22} \\ \epsilon_{12} \end{pmatrix} \tag{1}$$

where the strains are defined by

$$\epsilon_{ij} = \frac{1}{2}\left(\frac{\partial u_i}{\partial x_j} + \frac{\partial u_j}{\partial x_i} + \sum_l \frac{\partial u_l}{\partial x_i}\frac{\partial u_l}{\partial x_j}\right), \quad (i,j=1,2), \tag{2}$$

which takes into account nonlinear components of the strain tensor. The stress-equilibrium equation in absence of body forces is,

$$\mathbf{D}^T\sigma = \mathbf{0}, \tag{3}$$

where

$$\mathbf{D} = \begin{pmatrix} \frac{\partial}{\partial x_1} & 0 \\ 0 & \frac{\partial}{\partial x_2} \\ \frac{\partial}{\partial x_2} & \frac{\partial}{\partial x_1} \end{pmatrix} \quad \text{and} \quad \sigma = \begin{pmatrix} \sigma_{11} \\ \sigma_{22} \\ \sigma_{12} \end{pmatrix}. \tag{4}$$

The equations (1) – (3) for nonlinear components of the strain tensor ϵ, give rise to a system of nonlinear partial differential equations for the unknown displacements, u_1 and u_2.

In the above equations, σ_{11} and σ_{22} are normal stresses, τ_{12} is shear stress, u_i is the displacement in the i directions, ϵ_{11} and ϵ_{22} are normal strains, ϵ_{12} is shear strain, E_1 and E_2 are Young's Moduli along principal directions of elasticity, also known as axes of symmetry [27] which depend upon the position of anatomical fibers, ν_1 and ν_2 are Poisson's ratio (subject to $\nu_1 E_2 = \nu_2 E_1$) and G is the shear modulus. It may be mentioned that although a linear stress-strain relationship with nonlinear components of strain tensor is used, the method of experimental loading, based on applying small steps of strain and stress relaxation, results in exhibiting a typical behavior of a nonlinear elastic material [22]. This type of incremental approach is a popular technique for taking into account the nonlinear aspects [5]. We take advantage of the experimental loading technique used by Reihsner et al. (1995) in our finite element procedure (ABAQUS) [11] to exhibit nonlinear behavior of skin. This procedure is accomplished using a standard finite element technique and when specified, a standard finite element technique in conjunction with infinite elements.

We assume the wound to be small compared to the size of computational region. We take the principal directions of elasticity [27] for the orthotropic skin to coincide

with the axes of the incised wound. We solve these problems having symmetrical and non symmetrical boundaries by using the finite element method [28] in conjunction with infinite elements. All simulations were performed in ABAQUS version 6.2-3 [11] on a Silicon Graphics R5000, OS 6.5-5.

The principal stresses, σ_1 and σ_2 which are of physiological interest [4] are given by

$$\sigma_1 = \frac{\sigma_{11} + \sigma_{22}}{2} + \frac{1}{2}\left[(\sigma_{11} - \sigma_{22})^2 + 4\tau_{12}^2\right]^{1/2}, \tag{5}$$

$$\sigma_2 = \frac{\sigma_{11} + \sigma_{22}}{2} - \frac{1}{2}\left[(\sigma_{11} - \sigma_{22})^2 + 4\tau_{12}^2\right]^{1/2}, \tag{6}$$

and are computed in the deformed configuration. The principal average stress index for principal stress σ_i is defined as the integral of σ_i over the computational area divided by this area [10].

The units of the incremental elastic parameters for abdominal skin in (1) as evaluated by Reihsner et al. (1995) are Nmg^{-1}. The traditional unit of stress is force/area; i.e., $\mathrm{N/m}^2$. Hence, we use the modified values of the elastic parameters for abdominal skin as previously reported [9, 10]. Thus we take $E_1 = 4.168\ \mathrm{N/m}^2$, $E_2 = 2.500\ \mathrm{N/m}^2$, $G = 0.694\ \mathrm{N/m}^2$, $\nu_1 = 0.498$ and $\nu_2 = 0.299$.

2.1 Infinite elements

The finite element technique is an effective and efficient method used to obtain solutions to boundary value problems [28]. For this reason, finite elements perform best on computations within a finite boundary. Hence, if the region of interest is small compared to the physical region, there is a need to utilize infinite elements to approximate the far field region. This approach uses infinite elements defined over semi-infinite domains with suitably chosen decay functions [11].

We assume the solution in the far field of the surrounding medium to be linear. For this model, the infinite element method is based on modelling the basic solution variable, u with respect to spatial distance r measured from a "pole" of the solution, so that $u \to 0$ as $r \to \infty$, and $u \to \infty$ as $r \to 0$ [11]. The description below which follows the derivation in the ABAQUS Theory Manual [11], will be brief.

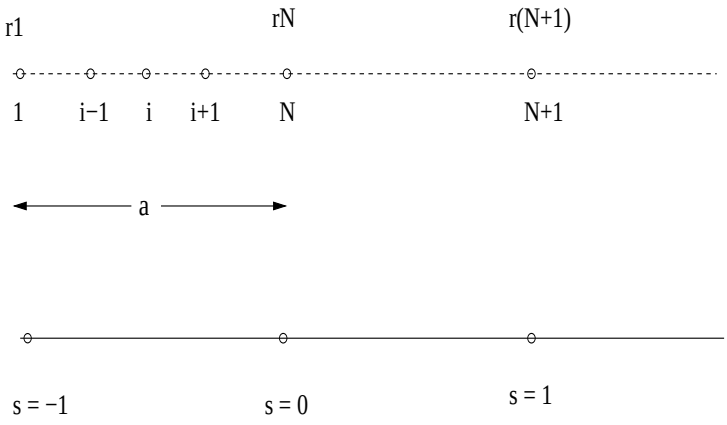

Figure 4: One dimensional finite and infinite element mesh. Nodes r_1 thru r_N comprise the finite element mesh, whereas nodes r_N and r_{N+1} define an infinite element.

Consider the following variables:

- r, distance away from the "pole." The "pole", corresponding to $r = r_0$, which is a distance a to the left of r_1 is omitted from Fig (4).
- s, the mapped coordinate variable corresponding to the distance r away from the pole such that $r(s)$ approaches infinity for s close to 1. That is,

$$r = -\frac{2s}{1-s} r_1 + \frac{1+s}{1-s} r_N. \tag{7}$$

- u, a quadratic Lagrange polynomial approximation that interpolates the solution $u(r(s))$ for $-1 \leq s \leq 1$.

Hence, we derive a mapping to ensure that $u = 0$ at $s = 1$, where $r \to \infty$. In one dimension, this reduces to $r = a$ defining node 1 corresponding to the finite boundary, $r = 2a$ defining node N, corresponding to the end of the mesh of finite elements, and $r = \infty$ corresponding to distances in the far field. This last node is represented by node $N + 1$. Simultaneously, we define our mapped variable s such that at node 1, $s = -1$, at node N, $s = 0$ and at node $N + 1$, $s = 1$. Thus

$$u = \frac{1}{2} s(s-1) u_1 + (1-s)(1+s) u_N \tag{8}$$

Combining equations (7) – (8) we obtain

$$u = (-u_1 + 4u_N)\frac{a}{r} + (2u_1 - 4u_N)\left(\frac{a}{r}\right)^2 \tag{9}$$

which is valid for $r_1 \leq r < \infty$.

In two dimensions, the method is extended by allowing each radial component of the mesh to be defined as in the one dimensional derivation (Fig 5). Specifically, nodes a_1 thru a_N and nodes b_1 thru b_N comprise the finite element mesh, whereas the four nodes b_N, a_N, a_{N+1} and b_{N+1} define an infinite element.

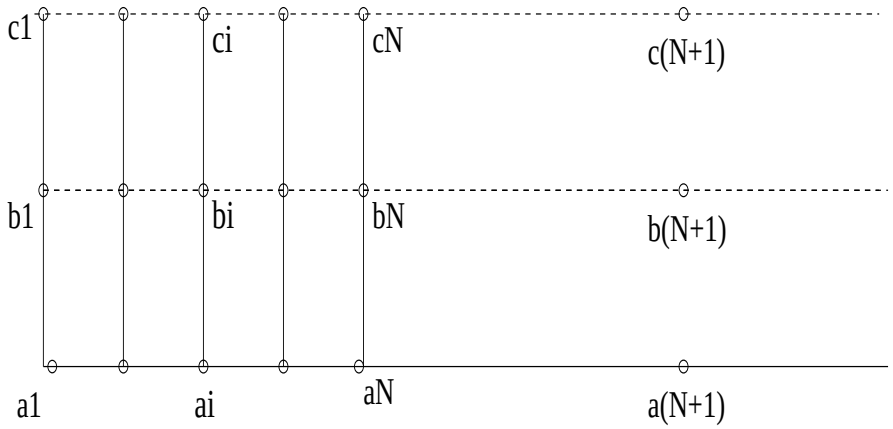

Figure 5: Two dimensional finite and infinite element mesh. Nodes a_1 thru a_N and nodes b_1 thru b_N comprise the finite element mesh, whereas the four nodes b_N, a_N, a_{N+1} and b_{N+1} define an infinite element.

3 Numerical Results

The use of infinite elements to compute the optimal patterns for wound closure based on stress analysis is a remarkable improvement over traditional finite element simulations and yields quantitatively and qualitatively accurate results.

In the first part of problem one, the average principal stresses σ_1 and σ_2 and the displacement, u (at the outer boundary), are determined as a result of suturing the circular wound in a finite skin sheet (Figs (6a) – (6b)). The maximum principal stress σ_1 occurs in a small (elliptical like) region about the center of the suture line. Compressive stresses occur at the ends of the suture line since the skin is *pushed out* at the ends when the vertical suturing occurs. These maximum compressive stresses are double the magnitude of the maximum tensile stresses.

For each successive computation, i, the number of elements of the computational region was increased while the number of elements in the control region remained at 440 (Table I). Meshes containing radial lengths of elements equal to 11, 14, 19, 24, 29, 39, 49, 74, and 99 were considered.

As expected, the value of the principal stress σ_1 continues to decrease as the artificial boundary is moved further away from the wound itself. We obtain significant percent changes in the principal stresses σ_1 and σ_2 which indicates that the solution is sensitive to modifications in the mesh size. Note that for a computationally expensive mesh of 3960 elements, the value of σ_1 is still a 0.42 percent change from the previous calculation with 2960 elements. Since the value of the average principal stress σ_1 is reported to be 0.092 in Chaudhry et al. [10] and we obtain a value of 0.09146, these results are close enough to consider the simulations accurate. Changes in displacement range from 16 - 33 % in magnitude suggesting the displacement drops significantly as the artificial boundary is enlarged. Note that the simulations converge to the same solution.

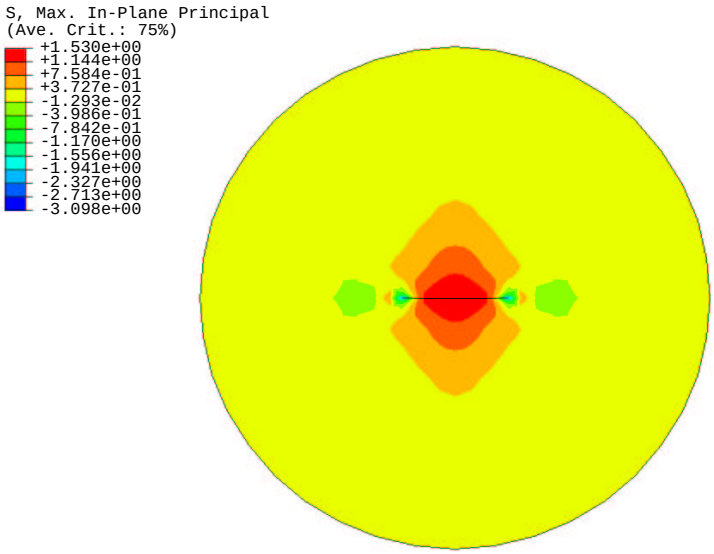

Figure 6a: Maximal principal stress σ_1, post-suturing, for a circular wound of orthotropic, abdominal human skin. Computational mesh of 440 isoparametric finite elements cover the region Ω_0. Area of the circular region is 9.4×10^{-4} m^2. σ_1 is largest (tensile) in a small region about the center of the suture line and decreases as it fans out radially. There are significant compressive stresses at the ends of the suture line which are double the magnitude of tensile stresses. Units of stress are N/m^2.

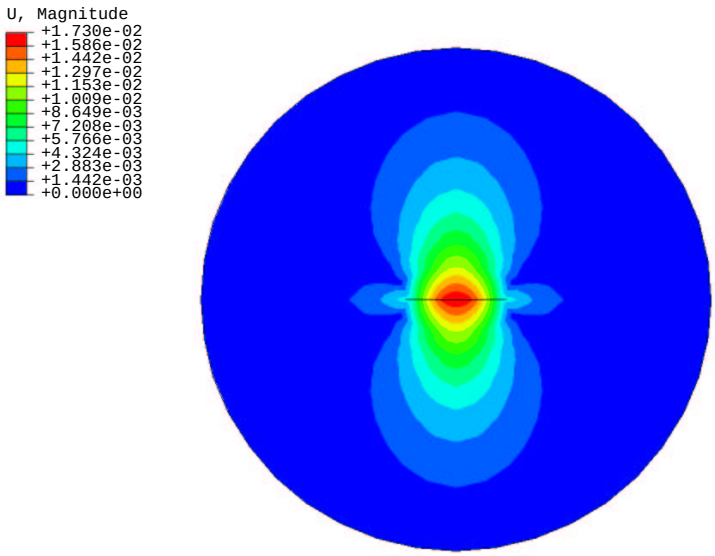

Figure 6b: Displacement, u, post-suturing, for a circular wound of orthotropic, abdominal human skin. Computational mesh of 440 isoparametric finite elements cover the region Ω_0. Area of the circular region is 9.4×10^{-4} m^2. u is largest in a small region about the center of the suture line and decreases as it fans out radially (vertically). Units of displacement in meters.

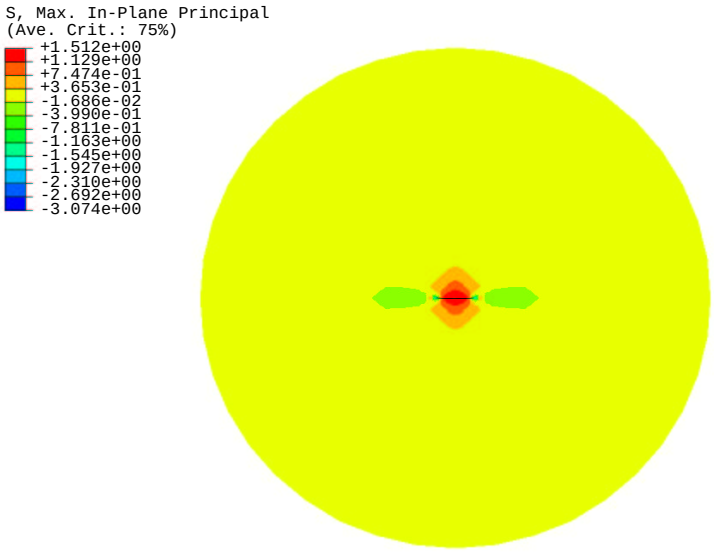

Figure 7a: Maximal principal stress σ_1, post-suturing, for a circular wound of orthotropic, abdominal human skin. Computational mesh of 440 isoparametric finite elements is surrounded by 40 infinite elements. Area of the circular region is 9.4×10^{-4} m^2. σ_1 is largest (tensile) in a small region about the center of the suture line and decreases as it fans out radially. There are significant compressive stresses at the ends of the suture line. Units of stress are N/m^2.

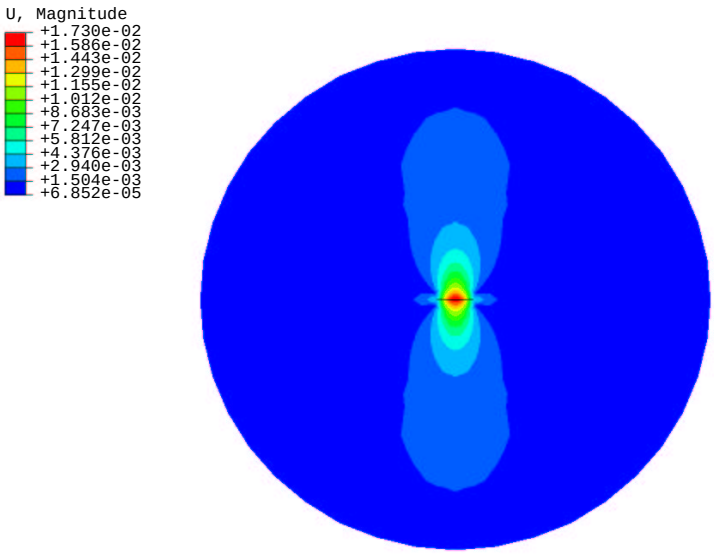

Figure 7b: Displacement u, post-suturing, for a circular wound of orthotropic, abdominal human skin. Computational mesh of 440 isoparametric finite elements surrounded by 40 infinite elements. Area of the circular region is 9.4×10^{-4} m^2. u is largest in a small region about the center of the suture line and decreases as it fans out radially (vertically). Units of displacement are in meters.

# of FE	Nodes	σ_1	% change	σ_2	% change	u	% change
440	480	12.63474		-3.06306		.21467	
560	600	11.37568	9.96506	-4.37375	42.78995	.17307	19.3787
760	800	10.35274	8.99234	-5.26825	20.45159	.12786	26.12419
960	1000	9.89818	4.39075	-5.74663	9.08041	.102721	19.65940
1160	1200	9.65251	2.48200	-6.01092	4.59898	.085860	16.41455
1560	1600	9.40837	2.52920	-6.27938	4.46626	.064687	24.66011
1960	2000	9.29567	1.19794	-6.40614	2.01863	.051875	19.80565
2960	3000	9.18459	1.19492	-6.53431	2.00072	.034732	33.04761
3960	4000	9.14550	0.42558	-6.57962	0.69350	.026112	24.82020

Table I: Results from the closure of a circular wound via finite elements (FE) only. Current (deformed) area of the circular control region Ω_0 is 4.00315×10^{-2} which is approximated by a numerical mesh of 440 CPS4 finite elements and 480 nodes. Principal stresses, σ_1 and σ_2 and displacement, u, are in units times 10^{-2}.

In the second part of problem one, we obtain significant improvements to the approximation of the average principal stress σ_1 with a mesh containing only 480 elements (440 finite elements and 40 infinite elements on the boundary) (Table II). Figures of average principal stress σ_2 have been omitted due to space limitations (Figs (7a) – (7b)). Similar distributions occur for principal stresses σ_1 and σ_2 as in the calculations with finite elements only. Note that the displacements die out at a faster more natural rate due to the removal of zero displacement boundary restrictions.

With each successive simulation that increases the area of the computational region by adding elements radially to the mesh, we obtain extremely small changes in the calculation of average principal stresses. In particular, calculations with a mesh containing 560 finite elements and 40 infinite elements provides a 0.004 percent improvement over the coarser mesh of 440 finite elements and 40 infinite elements. Since the percent change of the solution decreases rapidly with successive simulations, we conclude that these computations become mesh independent, are quantitatively accurate and suggest that the average principal stress σ_1 is around 9.095×10^{-2} N/m^2. Percent changes in displacement average around 10% with each simulation. Hence, the magnitude of the displacements continue to drop significantly with larger approximations of the far field region.

In problem one, we assumed that the boundary of the circular sheet enclosing the circular wound is a circle. Similarly, in problem two, we can choose the boundary of the elliptical sheet enclosing the elliptical wound to be an ellipse, in addition to an elliptical control region, Ω_0.

Ω_0 is covered by a computational mesh of 440 isoparametric finite elements. In each simulation, i, the far field region is approximated by a mesh of 40 infinite elements on the boundary of Ω_i. Wound closure simulations with increasing area of Ω_i yield average principal stresses of 5.16844×10^{-2} N/m^2 which differs significantly from the results reported in Chaudhry et al. [10] by 23 %. Chaudhry et al. [10] however, assume that

# of FE	Nodes	σ_1	% change	σ_2	% change	u	% change
440	520	9.10278		-6.63265		.031643	
560	640	9.09872	0.04455	-6.63604	0.05108	.028148	11.04763
760	840	9.09661	0.02317	-6.63800	0.02950	.024253	13.83770
960	1040	9.09567	0.01039	-6.63868	0.01027	.02163	10.81343
1160	1240	9.09538	0.00319	-6.63896	0.00422	.01971	8.88041
1560	1640	9.09520	0.00203	-6.63917	0.00312	.01703	13.59019
1960	2040	9.09508	0.001293	-6.63923	0.00104	.01521	10.67163
2960	3040	9.09499	0.00101	-6.63929	0.00081	.01240	18.49020
3960	4040	9.09497	0.00012	-6.63930	0.00025	.01073	13.46974

Table II: Results from closure of a circular wound via finite (FE) and infinite (IE) elements. Current (deformed) area of the circular control region Ω_0 is 4.00315 $\times 10^{-2}$ which is approximated by a numerical mesh of 440 CPS4 finite elements 40 CINPS4 infinite elements are added on the perimeter of Ω_0 to comprise the mesh of Ω_i. Principal stresses, σ_1 and σ_2 and displacement, u are in units times 10^{-2}.

the control region Ω_0 is a square of dimensions 0.2m by 0.2m for each geometry and closure pattern evaluated. Here, we do not obtain the same value of principal stresses even though our results yield a solution which eventually is mesh size independent. In order to make a quantitative comparison of this problem, each simulation is repeated in a square computational region meshed by 440 finite elements and 40 infinite elements for the circular and elliptical wounds. These simulations are computed in problem three.

In the third problem, we compare the average principal stresses resulting from closure of circular, elliptical and cardioid shape wounds on a square region Ω_0 of undeformed area 4.0×10^{-2} m^2. First, we suture a cardioid shaped region in several different patterns. We determine the optimal placement of the suture line to be at $y = 0.006$ of all the sample lines tested (Table III). This conclusion is based on the minimum value of the average principal stress σ_1 of 8.64188×10^{-2} N/m^2. The process of moving the suture line to determine the optimal suturing pattern could be useful to the surgeon faced with the problem of deciding in which manner one should suture a specific wound.

Note that more accurate definitions of the suture line could be obtained by taking a larger number of test lines. Figs (8a) – (8b) depict stress and displacement profiles post-suturing for average principal stress σ_1 and displacement, u, respectively. Average principal stress σ_1 is largest (tensile) in a very small region about the center of the suture line. There are significant compressive stresses at the ends of the suture line. These compressive stresses are not double the maximum tensile stresses as in the simulation of the circular wound, but are much less. Figures of average principal stress σ_2 have been omitted due to space limitations.

The circular wound is again closed but now it is within the square region. Fig (9) depicts the maximal principal stress σ_1, post-suturing, for a circular wound of orthotropic, abdominal, human skin. σ_1 is largest (tensile) in a small region about the center of the

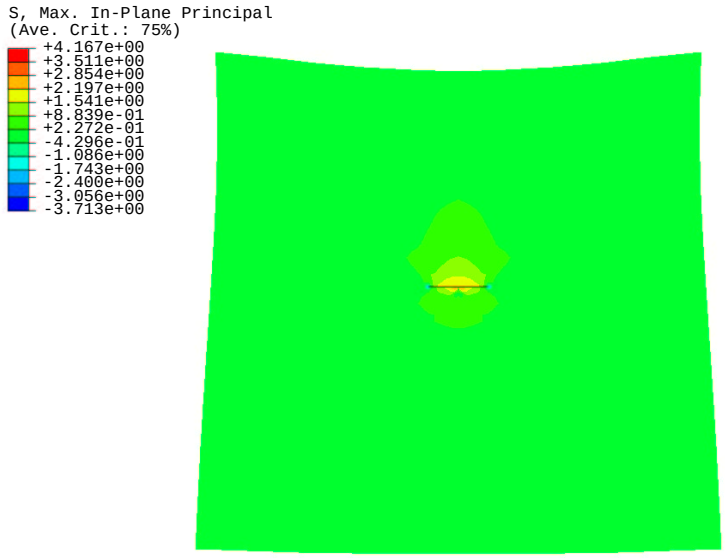

Figure 8a: Maximal principal stress σ_1, post-suturing, for a cardioid wound of orthotropic, abdominal human skin. Computational mesh of 360 isoparametric finite elements surrounded by 40 infinite elements. Area of the cardioid region is 9.4×10^{-4} m^2. σ_1 is largest (tensile) in a very small region about the center of the suture line. There are significant compressive stresses at the ends of the suture line. Units of stress are N/m^2.

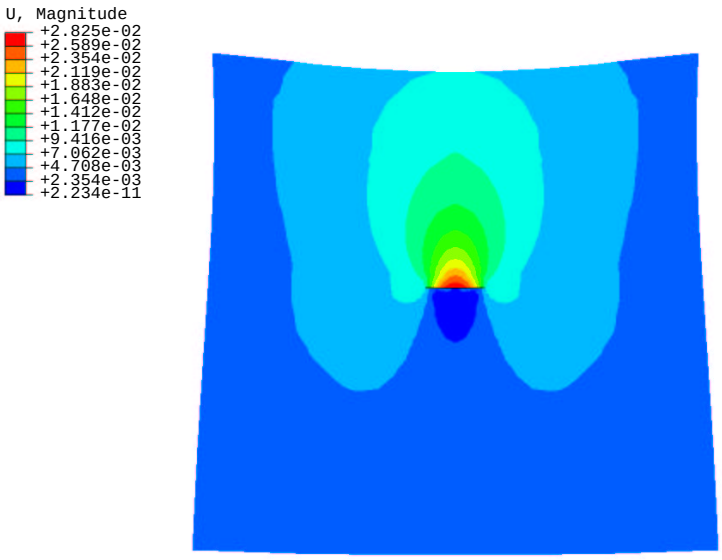

Figure 8b: Displacement, u, post-suturing, for a cardioid wound of orthotropic, abdominal human skin. Computational mesh of 360 isoparametric finite elements surrounded by 40 infinite elements. Area of the cardioid region is 9.4×10^{-4} m^2. u is largest in a region comprising approximately 2/3 of the suture line in the center and is significant above the suture line where displacements are the greatest. Units of displacement are in meters.

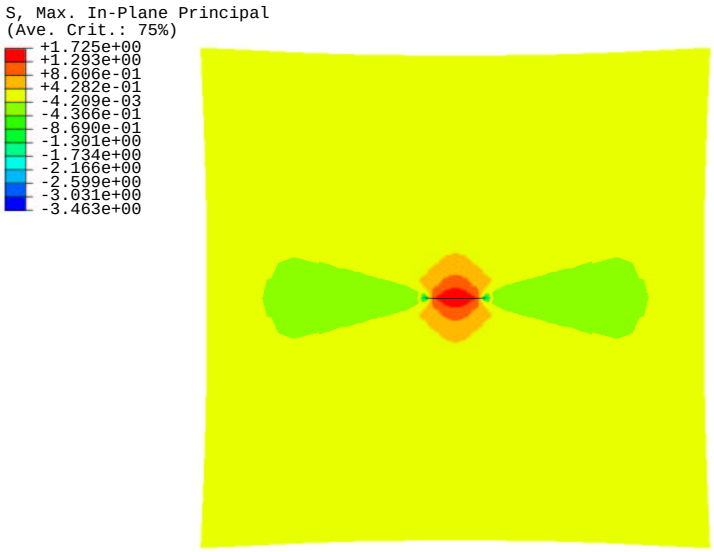

Figure 9: Maximal principal stress σ_1, post-suturing, for a circular wound of orthotropic, abdominal human skin. Computational mesh of 440 isoparametric finite elements surrounded by 40 infinite elements. Area of the circular region is 9.4×10^{-4} m^2. Deformed area of the square region Ω_0 is 3.90639×10^{-2} m^2. σ_1 is largest (tensile) in a small region about the center of the suture line and decreases as it fans out radially. There are significant compressive stresses at the ends of the suture line. Units of stress are N/m^2.

y-line	σ_1	σ_2	u
0.000	8.91929	-6.45068	.98657
0.004	8.69102	-6.19093	.77754
0.006	8.64188	-6.11311	.65344
0.007	8.68026	-6.17621	.64896
0.008	8.65848	-6.15382	.60465
0.012	8.67980	-6.04507	.39059
0.016	8.67980	-6.04507	.39059
0.020	9.37340	-6.35763	.88124
0.024	9.95385	-6.68155	1.07525

Table III: Results from closure of a cardioid wound via finite and infinite elements. Of the sample tested, minimum principal stresses occur when the suturing line is located at $y = 0.006$. Reference area of square control region Ω_0 is 4.0 $\times 10^{-2}$ and current area of Ω_0 is 3.90677×10^{-2}. Computational region is approximated by a numerical mesh of 360 CPS4 finite elements, 40 CINPS4 infinite elements on the perimeter of Ω_0 and 480 nodes. Principal stresses, σ_1 and σ_2 and displacement, u are in units times 10^{-2}.

suture line and decreases as it fans out radially. There are significant compressive stresses at the ends of the suture line.

Fig (10) depicts the maximal principal stress σ_1, post-suturing, when an elliptical wound of orthotropic, abdominal human skin is closed in the square region, Ω_0. σ_1 is largest (tensile) in a small region of narrow height about the center of the suture line and decreases as it fans out vertically. There are significant compressive stresses at the ends of the suture line but these are only 1/3 the magnitude of the maximum tensile stresses.

Wound Shape	Current Area of Ω_0	σ_1	σ_2	u
Circle	3.90639	9.11738	-6.53520	.388581
Ellipse	3.90638	6.70786	-4.03881	.393784
Cardioid	3.90677	8.64188	-6.11312	.653442

Table IV: Results from closure of wounds via finite and infinite elements. Reference area of square control region Ω_0 is 0.04 m^2. Current area (after deformation) of Ω_0 is displayed in column 2. Area of open wound is 9.4×10^{-4} m^2 for all geometries. Principal stresses, σ_1 and σ_2 and displacement, u, are in units times 10^{-2}.

With the square control mesh, the value of principal stress σ_1 is 9.11737×10^{-2} Nm/s^2 and to two decimal places, is almost exactly the value of 0.092 as previously reported for closure of the circular wound. The values of average principal stress σ_1 for the ellipse were also quantitatively accurate (Table IV) as compared to stresses computed analytically [10].

These numerical results agree with the analytical results of Chaudhry et al. [10] which conclude that suturing of the elliptical wound results in the lowest principal stresses. In

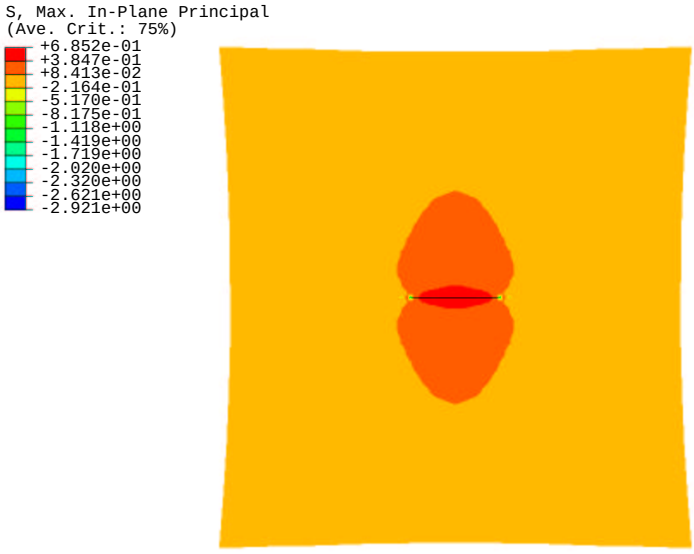

Figure 10: Maximal principal stress σ_1, post-suturing, for an elliptical wound of orthotropic, abdominal human skin. Computational mesh of 440 isoparametric finite elements surrounded by 40 infinite elements. Area of the elliptical region is 9.4×10^{-4} m^2. Deformed area of the square region Ω_0 is 3.90638×10^{-2} m^2. σ_1 is largest (tensile) in a small region of narrow height about the center of the suture line and decreases as it fans out vertically. There are significant compressive stresses at the ends of the suture line but these are only 1/3 the magnitude of the maximum tensile stresses. Units of stress are N/m^2.

addition, we conclude that the cardioid is a preferred closure geometry over the circle, although not optimal. Most significantly, these results *quantitatively* agree with the analytical results of Chaudhry et al., 1998 [10] and now suggest that this numerical technique is both quantitative and qualitatively correct.

4 Discussion

As hypothesized and shown in [10], the optimal suturing pattern of problems 1, 2 and 3 is the elliptical shaped wound sutured toward the major axis. These results were obtained after careful quantitative analysis of optimal closure patterns based on stress analysis using both finite and infinite element meshes. Of vital interest is the precision in which actual values of principal stresses match predicted values computed using complex variable techniques.

Although the solutions are greatly improved by the addition of infinite elements, these models still depend upon simulations computed with finite elements only. In particular, one must exhibit caution when choosing the domain Ω_0. Numerical simulations computed with finite elements only should be evaluated to determine the minimum size of Ω_0 for which the solution no longer changes with respect to increasing boundary conditions. If the computational mesh of Ω_0 ignores areas of the surrounding medium which influence the stress distribution locally around the wound, the average principal stresses computed will be underestimated. Hence, the area of region Ω_0 should be chosen as the minimum area that will enclose the wound and regions contributing to local stresses.

Moreover, we theorize that the region Ω_0 is best chosen to be of the same geometry as the wound since stresses which develop as a result of suturing are dependent on the shape of the wound edge. Thus, the finite element technique is useful in defining the shape of the control region Ω_0. Since, however, the region of interest is small compared to the surrounding medium but influenced by this medium, infinite elements should be used in conjunction with finite elements in order to achieve quantitatively accurate solutions.

Lastly, this technique should greatly improve the computation of stresses resulting from suturing in three dimensions. This application is the subject of future study.

5 Conclusion

Accurate quantitative results are obtained when solid infinite elements are used in conjunction with finite elements to compute stress and displacement distributions resulting from the suturing of wounds in orthotropic, abdominal, human skin. If one seeks to choose an optimal pattern of suturing based on break strength of wounds, any model which is based upon finite elements only and does not incorporate infinite elements will incorrectly estimate the maximum stresses due to suturing. These results are informative to the surgeon who wishes to close nonsymmetric wounds on regions of the body that exhibit orthotropy.

Acknowledgments

This work was supported in part by the National Science Foundation DMS-9803605 and the Foundation at the New Jersey Institute of Technology. The authors thank the Center for Applied Mathematics and Statistics, the Department of Mathematical Sciences and the Biomechanical Engineering Department at N.J.I.T. for research facilities.

References

[1] Bucalo, B.D., Iriondo, M., 1995. Photoelastic models of wound closure stress. *Dermatol. Surg.* **21**, 210 – 212.

[2] Cacou, C., Muir, I.F.K., 1995. Effects of plane mechanical forces in wound healing in humans. *J. R. Coll. Surg. Edinb* **40**, 38 – 41.

[3] Gibson, T., 1990. Physical properties of skin. In Plastic Surgery, Vol. 1 General Principles. W. B. Saunders Co., Philadelphia, p. 123.

[4] Danielson, D.A., Natrajan, S., 1975. Tension field theory and the stress in stretched skin. *J. Biomechanics* **8**, 135 – 142.

[5] Fung, Y.C. *Biomechanics*, Springer Verlag, Berlin 1984, 196 – 260.

[6] Tong, P., Fung, Y.-C., 1976. The stress-strain relationship for the skin. *Journal of Biomechanics* **9**, 649 – 657.

[7] Larrabee, W.F., Holloway, G.A., Sutton, D., 1984. Wound tension and blood flow in skin flaps. *Annals of Otol. Rhinol. Laryngol.* **93**, 112 – 115.

[8] Larrabee, W.F., Galt, J.A., 1986. A finite element model of skin deformation. III. The finite element model. *Laryngoscope* **96**, 413 – 419.

[9] Lott-Crumpler, D.A., Chaudhry, H.R., 2001. Optimal patterns for suturing wounds of complex shapes to foster healing. *J. Biomechanics* **34**, 51 – 58.

[10] Chaudhry, H.R., Bukiet, B., Siegel, M., Findley, T., Ritter, A.B., Guzelsu, N., 1998. Optimal patterns for suturing wounds. *J. Biomechanics* **31**, 653 – 662.

[11] Hibbitt, Karlsson & Sorensen, Inc., Getting Started with ABAQUS/Standard, 1996.

[12] Ihlenburg, F., 2000. On fundamental aspects of exterior approximation with infinite elements. *J. Comput. Acoustics* **8**(1), 63 – 80.

[13] Burnet, D. S., 1997. Overview of multipole-based acoustic infinite elements. ASA 134^{th} Meeting, San Diego, California.

[14] Dreyer, D. Hydrodynamic loads on offshore structures.
http://uranus.mt2.tu-harburg.de/ddreyer/project.html is the HTTP address.

[15] Al Salemeh, M. S., Alkhawaldeh, S. A., 2000. Computer modeling of optical dielectric waveguides by edge infinite elements. *J. Optical Comm.* **21**(2)

[16] Simoni, L. and Schrefler, B.A., 1987. Mapped infinite elements in solid consolidation. *Int. J. N.M.E.* **25**, 513 - 527.

[17] Yerli, H.R., Temel, B., Kiral, E., 1998. Transient infinite elements for 2D soil-structure interaction analysis. *J. Geotech. Geoenviron. Eng.* **124** (10), 976 – 988.

[18] Silvester, P.P., Hsieh M.S., 1971. Finite-element solution of 2-dimensional exterior-field problems. Proceedings of the Institution of Electrical Engineers, **118**, 1743 – 1747.

[19] Kagawa, Y., Murai T., Kitagami, S., 1982. On the compatibility of finite element-boundary element coupling in field problems. COMPEL - *Int. J. Comput & Math. in Electrical & Electronic Engineering* **1**, 197–217.

[20] Silvester, P.P., Lowther, D.A., Carpenter, C.J., Wyatt, E.A., 1977. Exterior finite elements for 2-dimensional field problems with open boundaries. Proceedings of the Institution of Electrical Engineers, **124**, 1267–1270.

[21] Lowther, D. A., Rajanathan C.B., Silvester, P.P., 1978. A finite element technique for solving 2-D open boundary problems. *IEEE Transactions on Magnetics* **MAG-14**, 467-469.

[22] Reihsner, R., Balogh, B., Menzel, E.J., 1995. Two-dimensional elastic properties of human skin in terms of an incremental model at the *in vivo* configuration. *Med. Eng. Phys* **17**, 304 – 313.

[23] Christensen, M.S., Hargens III, C.W., Nacht, S., Gans, E.H., 1977. Viscoelastic properties of intact human skin: instrumentation, hydrations effects, and the contribution of the stratum corneum. *J. Investigative Dermat.* bf 69 282 – 286.

[24] Har-Shai, Y., Bodner, S.R., Egozy-Golan, D.i, Lindenbaum, E.S., Ben-Izhak, O., Mitz, V., Hirshowitz, B., 1997. Viscoelastic properties of the Superficial Muscoluaponeurotic System (SMAS): A microscopic and mechanical study. *Aesth. Plast. Surg.* **21**, 219 – 224.

[25] Rubin, M.B,, Bodner, S.R., Binur, N.S., 1998. An elastic-viscoplastic model for excised facial tissues. *J. Biomechanical Engineering* **120**, 686 – 689.

[26] Rubin, M.B., Bodner, S.R., 2001. *Int. J. Solids Structures*, to appear.

[27] Lekhnitskii, S.G., 1981. Theory of elasticity of an anisotropic body. Mir Publishers, Moscow (Translation from Russian.)

[28] Zienkiewicz, O.C., Taylor, R., 1989. The finite element method, 4th Ed., Vol. 1. McGraw-Hill.